American Journal of Physical Chemistry
2025, Vol. 14, No. 4, pp. 110–124
https://doi.org/10.11648/j.ajpc.20251404.13

Research Article

Selective Removal of Methylene Blue Using Cellulose-Based Imprinted Polymers from Agro-Waste

Chinyere Emmanuella Okafor[1, *], Collins Chinonso Osuagwu[1], Ekene Chidozie[2], Nnaemeka John Okorocha[3], Cynthia Chimaobi Onyeakazi[4], Obi Justina Nnenna[5], Anyiam Chiemelie Joel[5], Robert Enenmuo[1]

[1]Department of Pure and Industrial Chemistry, Chukwuemeka Odumegwu Ojukwu University, Uli, Nigeria

[2]Department of Chemistry, Admiralty University of Nigeria, Ibusa, Nigeria

[3]Department of Chemistry, Legacy University, Okija, Nigeria

[4]Department of Science Laboratory Technology, Federal University of Technology, Owerri, Nigeria

[5]Department of Chemistry, Federal University of Technology, Owerri, Nigeria

Abstract

Methylene blue (MB), a common cationic dye, poses environmental and health risks due to its persistence in industrial effluents. In this study, cellulose-based molecularly imprinted polymer (MIP) was synthesized from oil bean (*Pentaclethra macrophylla*) seed shell waste, using MB as a template. Non-imprinted polymer (NIP) was prepared as control. The materials were characterized by FTIR, SEM, and XRD, which confirmed successful polymerization and the presence of template-specific binding cavities in MIP. Batch adsorption experiments assessed the effects of pH, contact time, adsorbent dosage, initial dye concentration, and temperature. The adsorption kinetics followed a pseudo-second-order model, while equilibrium data were best fitted to the Freundlich isotherm, indicating heterogeneous surface binding. The maximum adsorption capacity of the MIP was 14.93 mg g^{-1}, compared with 10.26 mg g^{-1} for the NIP. Thermodynamic analysis showed the process was spontaneous and exothermic. Selectivity studies demonstrated strong molecular recognition of MB, with an imprinting factor of 3.37 and selectivity factors of 3.25 (MB/indigo carmine) and 2.89 (MB/fuchsin basic). These findings highlight that agro-waste valorization into functional MIPs provides an efficient and low-cost adsorbent with enhanced affinity and selectivity for dye removal. The study contributes to sustainable wastewater management by combining molecular imprinting with biomass utilization, thereby supporting circular economy goals. Future work should investigate regeneration, scale-up, and application in continuous-flow systems for practical deployment.

Keywords

Methylene Blue, Molecularly Imprinted Polymers, Cellulose, Oil Bean Shell, Agro-Waste Valorization, Wastewater Treatment

[*]Corresponding author: ellachinyere0@gmail.com (Chinyere Emmanuella Okafor)

Received: 20 September 2025; **Accepted:** 4 October 2025; **Published:** 26 December 2025

1. Introduction

Synthetic dyes are recognized as major industrial pollutants because of their chemical stability and toxicity. Methylene blue (MB), a cationic thiazine dye widely used in textiles, plastics, and paper industries, persists in aquatic systems and poses health risks including skin irritation, respiratory distress, and neurotoxicity [1, 2]. Conventional wastewater treatment methods such as coagulation, advanced oxidation, and membrane filtration are often constrained by poor efficiency at low concentrations, secondary pollution, and high operational costs [3, 4].

Adsorption has emerged as an effective and scalable strategy due to its simplicity, cost-effectiveness, and versatility [2, 5]. Activated carbon remains the benchmark adsorbent but is hindered by high regeneration costs, poor selectivity, and reduced efficiency after repeated use [6, 7]. Agricultural residues, clays, and biopolymers have been investigated as low-cost alternatives, yet their lack of molecular selectivity limits performance in complex effluents [1, 8-10].

Molecularly imprinted polymers (MIPs) provide a superior approach by introducing template-specific recognition sites during synthesis. When MB is used as a template, functional monomers interact through hydrogen bonding, π-π stacking, and electrostatic forces, followed by crosslinking to stabilize these interactions. Removal of the template generates cavities complementary in size, shape, and functionality to MB molecules, conferring enhanced selectivity, structural stability under harsh conditions, and reusability compared to conventional sorbents [6, 4].

Recent advances have emphasized sustainability by sourcing MIP matrices from agro-wastes, which are abundant, renewable, and environmentally benign [5, 7]. Oil bean seed shells (Pentaclethra macrophylla), a lignocellulosic biomass rich in cellulose, hemicellulose, and lignin, are widely available in West Africa but typically discarded as waste. Converting this biomass into a functional polymer matrix aligns with circular economy principles, simultaneously addressing waste management and water pollution [2, 1].

Although MIPs have been widely investigated for pharmaceuticals, pesticides, and small organic pollutants, no prior study has reported the development of MIPs derived from oil bean seed shells for the selective removal of MB [3, 6]. To address this gap, the objectives of this study are to: (i) synthesize MIP from oil bean seed shells using MB as template; (ii) characterize the resulting polymers using FTIR, SEM, and XRD; (iii) evaluate adsorption performance through batch studies (kinetics, isotherms, and thermodynamics); and (iv) assess selectivity relative to non-imprinted polymer (NIP) and benchmark literature adsorbents.

2. Materials and Methods

2.1. Materials

Analytical-grade reagents were used throughout: sodium hydroxide (NaOH, 98%), ammonium persulfate (APS, 98%), acrylic acid (AA, 99%), acrylamide (AM, 98%), N,N′-methylenebisacrylamide (MBA, 99%), methylene blue (MB, 99%), methanol (99.8%), and ethanol (99.5%). All chemicals were purchased from Sigma-Aldrich (Germany). Deionized water was used in all preparations. Oil bean (Pentaclethra macrophylla) seed shells were collected from Orie Ekwe Market, Imo State, Nigeria, washed, oven-dried at 60 ℃, and ground to <0.5 mm.

2.2. Cellulose Extraction from Biomass

Cellulose was extracted following alkali and bleaching treatments commonly applied for lignocellulosic biomass. The seed shell powder was treated with 5 wt% NaOH at 80 ℃ for 2 h to remove lignin and hemicellulose, washed to neutral pH, then bleached with a 1:1 v/v solution of glacial acetic acid and 30% H_2O_2 at 90 ℃ for 2 h. The resulting cellulose was washed and oven-dried at 60 ℃. Similar procedures have been reported for preparing cellulose from agricultural residue [11, 12].

2.3. Synthesis of Molecularly Imprinted Polymer (OB-MIPMB)

OB-MIPMB was prepared by free-radical polymerization using APS as initiator and MBA as crosslinker. 2 g of cellulose was dispersed in 50 mL deionized water under stirring. APS solution (2 mL, 0.1 g/mL) was added and stirred for 15 min at 25 ℃. A 10 mL aqueous solution containing 8 g AA, 2 g AM, 0.06 g MBA, and 0.1 g MB (template) was introduced. Polymerization was carried out at 60 ℃ for 24 h under a nitrogen atmosphere, following protocols adapted from cellulose-polymer hydrogel systems [11, 6, 13].

2.4. Synthesis of Non-imprinted Polymer (OB-NIP)

OB-NIP was synthesized under identical conditions without the MB template, serving as a control for evaluating imprinting efficiency and selectivity.

2.5. Template Removal

The resulting OB-MIPMB was washed with methanol/acetic acid (9:1 v/v) until no MB was detected at 660 nm using UV-Vis spectroscopy. The polymer was then neutralized with 0.1 M NaOH, dehydrated with ethanol, and oven-dried at 60 ℃. Template elution using acidified alcohol mixtures is widely applied to generate recognition sites in dye-imprinted polymers [13].

2.6. Particle Size Fractionation

Both OB-MIPMB and OB-NIP were sieved to obtain fractions in the 100-200 μm range. Particle size control has been shown to influence surface accessibility and adsorption efficiency in MIPs [6].

2.7. Characterization

1) FTIR spectroscopy (400-4000 cm^{-1}, 4 cm^{-1} resolution) was used to confirm functional group incorporation and template removal [1].
2) SEM (JEOL JSM-5610, 15 kV) was used to study surface morphology and the presence of template-induced cavities [9].
3) XRD (Cu Kα radiation, 10-50° 2θ range) was performed to assess crystallinity changes in the cellulose backbone after polymerization [6].

2.8. Batch Adsorption Experiments

Batch adsorption studies were conducted in 25 mL solutions containing 10 mg adsorbent under agitation (150 rpm). The effects of pH (3-9), contact time (0-120 min), MB concentration (20-100 mg/L), temperature (30-70 ℃), and adsorbent dosage (0.05-0.25 g) were investigated. Residual MB concentrations were determined by UV-Vis spectrophotometry at 660 nm. Adsorption capacity was calculated, and kinetic (First-order, Second-order, intra-particle diffusion), isotherm (Langmuir, Freundlich, Temkin), and thermodynamic models were applied to evaluate adsorption mechanisms, following recent studies on dye-imprinted polymers [6, 9, 14].

2.9. Selectivity Studies

Single-component experiments were carried out using methylene blue (MB), indigo carmine, and fuchsin basic (50 mg/L, 25 mL, pH 7, 25 ℃, 10 mg adsorbent) of evaluate selectivity of OB-MIPMB. Equilibrium concentrations were measured by UV-Vis at 660 nm (MB), 610 nm (indigo carmine), and 540 nm (fuchsin basic). The distribution coefficients ($Kd = qe/Ce$) was calculated for each dye, and imprinting factors ($IF = Kd.MIP/Kd.NIP$) were determined by comparison with the non-imprinted polymer. Selectivity factors ($\alpha = Kd.MB/Kd.competing\ dye$) were used to determine the preferential binding of MB over structurally similar dyes. These metrics are widely adopted in MIP studies to evaluate template-specific recognition and competitive adsorption performance [13, 6].

3. Results and Discussion

3.1. Characterization of MIP and NIP

FTIR Characterization

The FTIR spectra of OB-MIPMB and OB-NIP (Figure 1) displayed the characteristic absorption bands of cellulose-based polymers. A broad band at 3200-3600 cm^{-1} corresponds to O-H stretching vibrations of cellulose hydroxyl groups and adsorbed water molecules [11]. Peaks at 2900-3000 cm^{-1} are assigned to C-H stretching of aliphatic methyl and methylene groups [1, 15]. The band at 1650-1700 cm^{-1} indicates C=O stretching vibrations, confirming the successful incorporation of acrylic acid and acrylamide monomers into the cellulose matrix via graft copolymerization [16]. Additional bands at 1450-1500 cm^{-1} correspond to C-H bending vibrations, while absorptions in the 1000-1200 cm^{-1} region are due to C-O stretching of the cellulose backbone [17]. These spectral features collectively verify the successful synthesis of both molecularly imprinted and non-imprinted polymers.

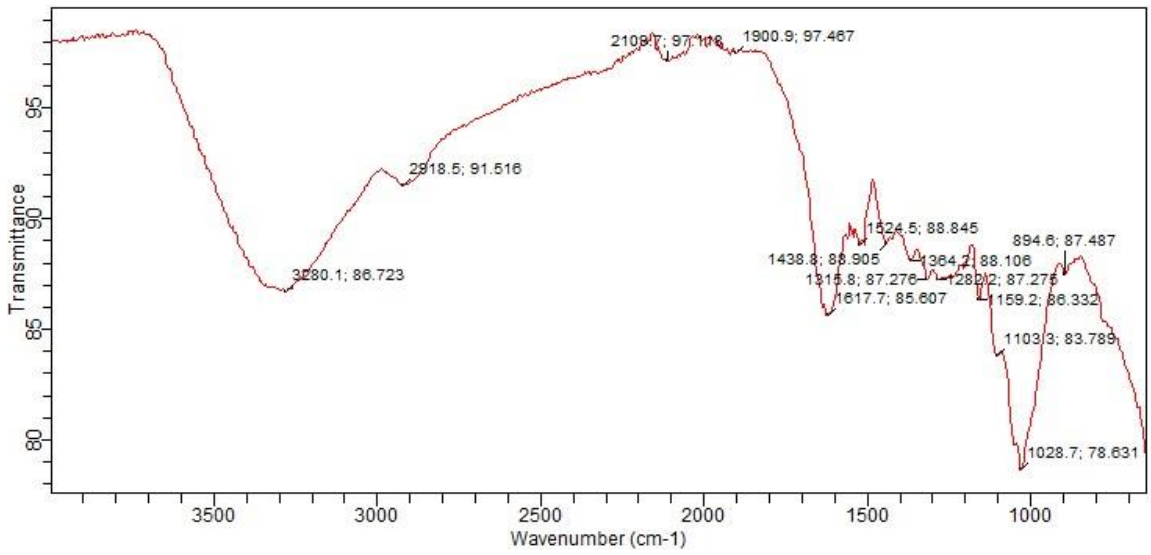

(a)

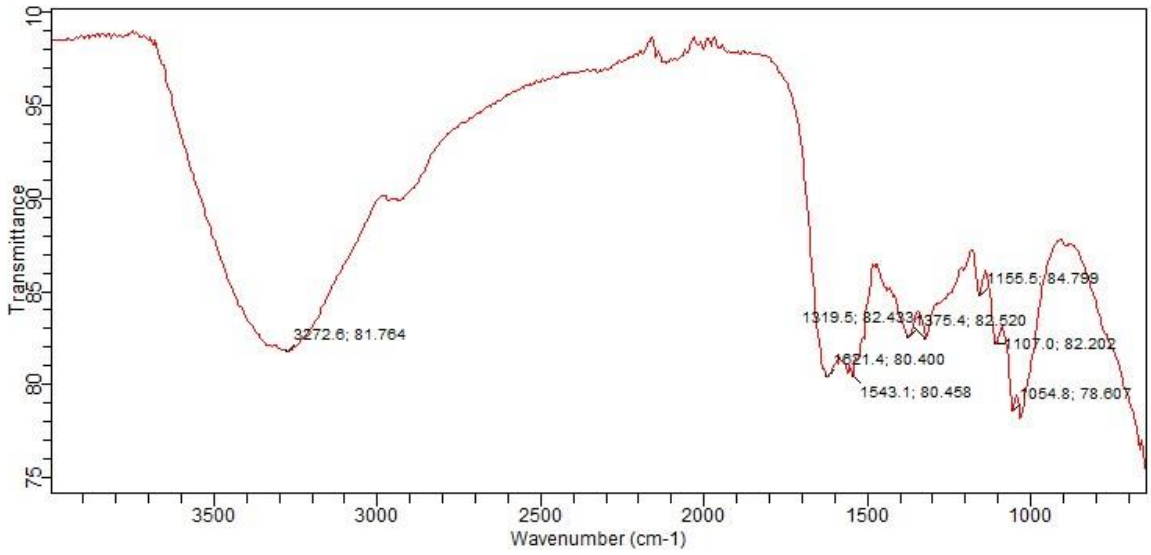

(b)

Figure 1. *FTIR Spectra of (a) OB-MIPMB and (b) OB-NIP.*

SEM Characterization

SEM micrographs (Figure 2) revealed clear morphological differences between OB-MIPMB and OB-NIP. The MIP exhibited a more porous and irregular surface with visible cavities and indentations, attributed to template removal during methylene blue extraction. These cavities correspond to molecular recognition sites, providing specific binding domains for target dye adsorption [6]. In contrast, the NIP surface appeared denser and more compact with fewer pores, reflecting the absence of template-guided imprinting. The enhanced porosity observed in the MIP aligns with previous studies on molecularly imprinted polymers, where template extraction produces selective cavities that increase surface roughness and accessibility [13, 17]. Such morphological modifications are critical for adsorption capacity, as higher porosity facilitates mass transfer and increases the number of available binding sites for dye molecules [15].

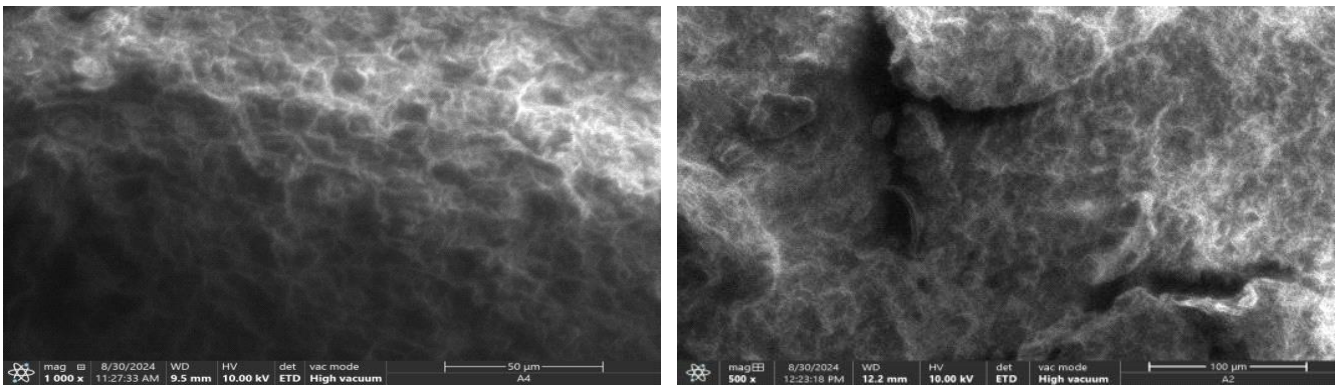

(a) (b)

Figure 2. *SEM Micrographs of (a) OB-MIPMB and (b) OB-NIP.*

XRD Characterization

The XRD patterns of OB-MIPMB and OB-NIP (Figure 3) displayed characteristic diffraction peaks of cellulose I, confirming that the crystalline structure of the biomass was largely preserved during polymerization. The main reflections at 2θ ≈ 16°, 22°, and 34° correspond to typical cellulose I crystallographic planes [18, 19]. A slight reduction in relative crystallinity was observed for OB-MIPMB compared to OB-NIP, calculated using the peak height (Segal) method. Such reduction is attributed to polymer grafting and template removal, which disrupts packing of microfibrils [20, 18]. Nevertheless, enough crystallinity remained to ensure structural stability, and the increased amorphous content likely enhanced accessibility of dye binding sites.

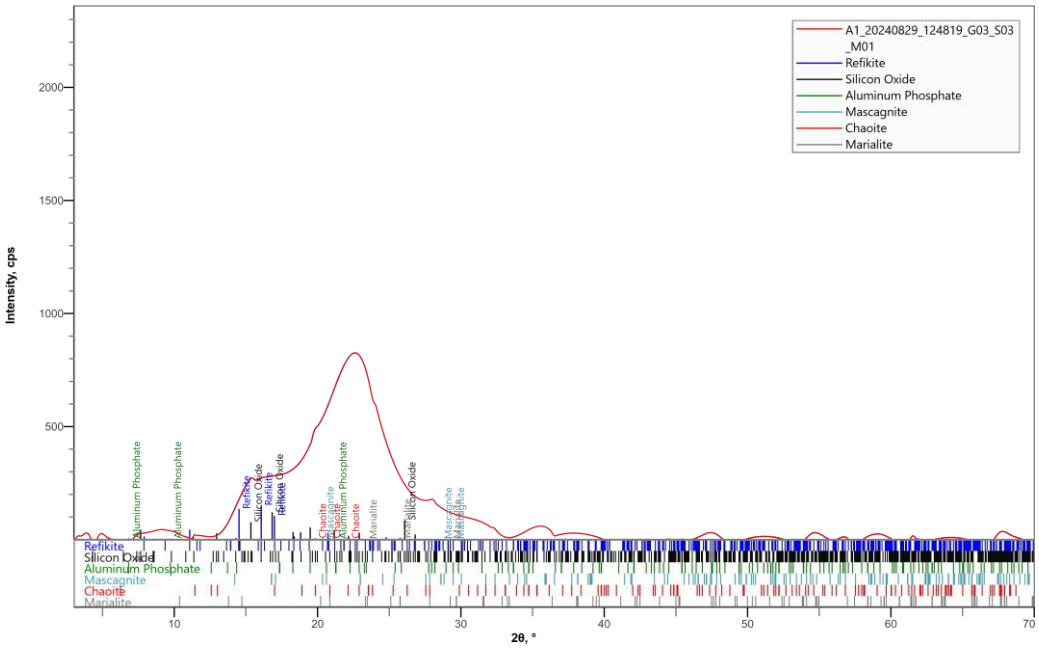

(a)

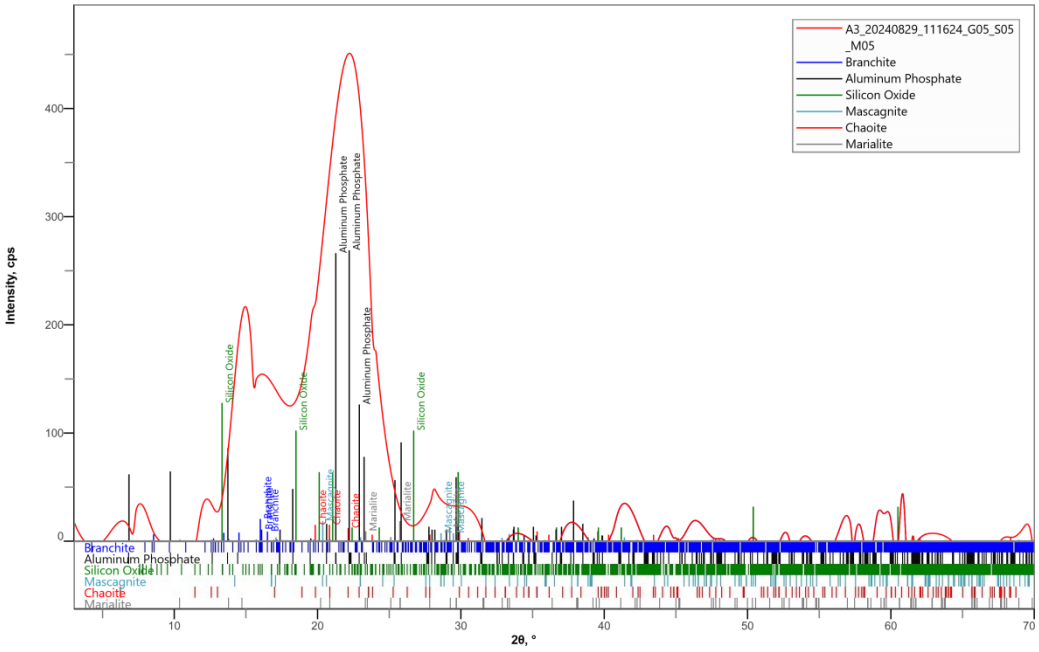

(b)

Figure 3. *XRD pattern of (a) OB-MIPMB (b) OB-NIP.*

3.2. Effect of Operational Parameters on Methylene Blue Adsorption

Effect of Contact Time

As shown in Figure 4 and Table 1, OB-MIPMB achieved higher MB removal (83.16%) than OB-NIP (59.42%) at equilibrium (120 min). Most adsorption occurred rapidly within the first 15 min (80.68% for MIP), reflecting abundant surface recognition sites created by imprinting, which enhance affinity and selectivity compared with nonspecific NIP sites [6, 13]. The subsequent slower uptake is attributed to intra-particle diffusion, yielding a typical two-phase profile of fast surface binding followed by gradual diffusion into pores, as reported for porous MIPs and cellulose-based adsorbents [16, 15].

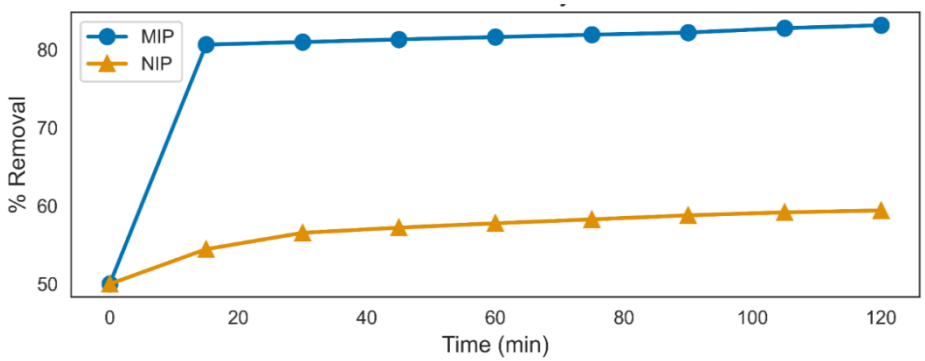

Figure 4. *Effect of contact time on MB adsorption by OB-MIPMB and OB-NIP.*

Effect of Adsorbent Dosage

As shown in Figure 5 and Table 1, MB removal increased with dosage for both adsorbents, but OB-MIPMB consistently outperformed OB-NIP (82.40% vs. 55.98% at 0.25 g). The modest efficiency gains at higher dosages indicate site saturation, consistent with Langmuir monolayer adsorption theory [16]. OB-MIPMB's consistently superior performance highlights the role of imprinting in generating high-affinity cavities, a trend also observed in other biomass-derived MIP systems [6, 13].

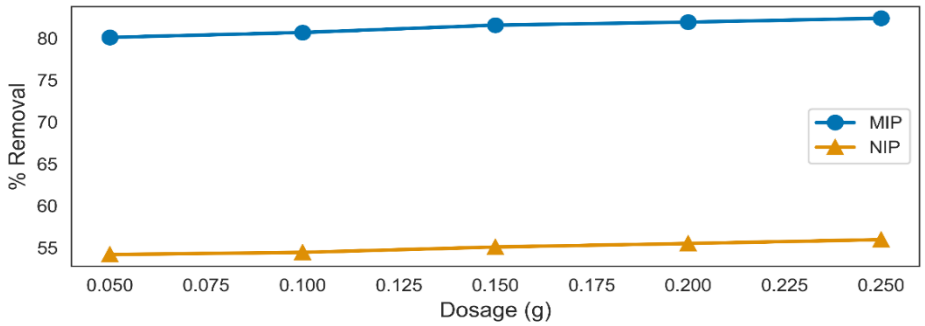

Figure 5. *Effect of adsorbent dosage on MB removal.*

Effect of Initial Concentration

As shown in Figure 6 and Table 1, OB-MIPMB achieved high MB removal at low concentrations (97.12% at 20 mg L^{-1}), which declined to 68.73% at 100 mg L^{-1}. OB-NIP performed less effectively, dropping from 71.35% to 58.73% across the same range. This inverse relationship between initial concentration and removal percentage is typical in adsorption, as finite binding sites become saturated at higher solute loads [15, 16]. At low concentrations, the ratio of available sites to dye molecules is favorable, enabling near-complete uptake, while higher concentrations exceed site capacity. The consistently superior performance of OB-MIPMB reflects the high-affinity cavities generated by imprinting, consistent with other dye-selective MIPs [6, 13].

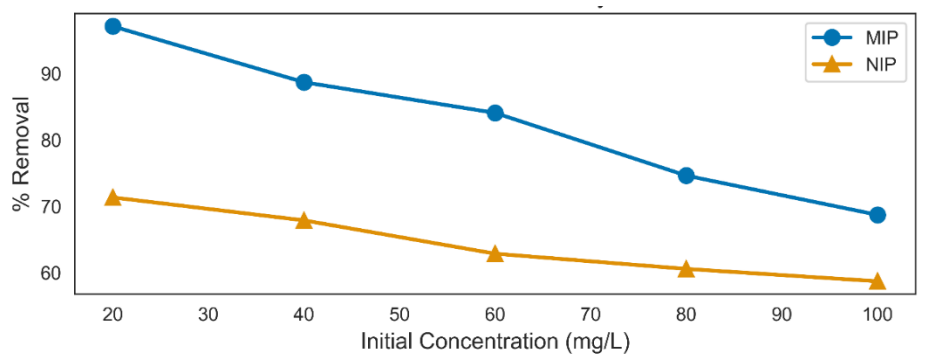

Figure 6. *Effect of initial MB concentration on adsorption efficiency.*

Effect of Temperature

Figure 7 and Table 1 shows that MB removal by OB-MIPMB decreased slightly from 80.70% at 303 K to 79.34% at 343 K, while OB-NIP declined from 56.46% to 54.26% over the same range. The reduction with rising temperature indicates an exothermic process, as increased thermal energy weakens dye-adsorbent interactions and promotes desorption [15, 16]. Such negative temperature dependence is characteristic of physical adsorption involving van der Waals forces, hydrogen bonding, and electrostatic interactions, which are less stable at elevated temperatures [5]. OB-MIPMB retained higher stability than OB-NIP across the tested range, reflecting the stronger affinity of imprinting-derived recognition sites, a trend consistent with other MIP-based dye adsorbents [6, 13].

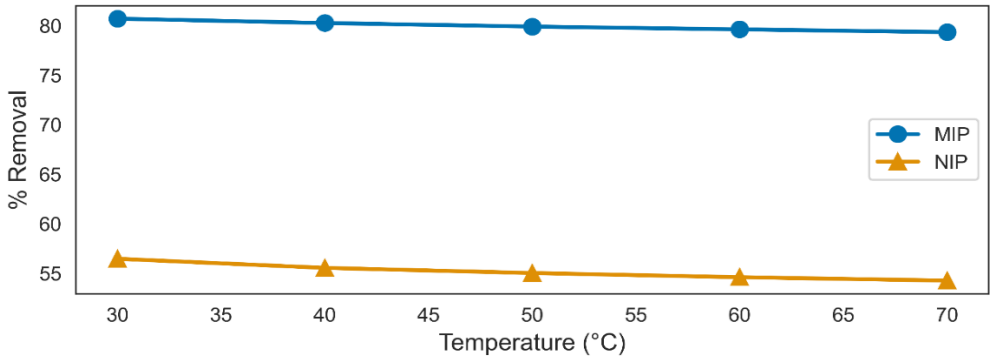

Figure 7. *Effect of temperature on MB adsorption.*

Effect of pH

Figure 8 and Table 6 show that OB-MIPMB maintained stable adsorption across pH 3-9 (80.32-81.06%), while OB-NIP consistently performed lower (54.18-54.82%). The slight decline at alkaline pH likely reflects electrostatic repulsion between the negatively charged polymer surface and deprotonated functional groups, which weakens dye-adsorbent interactions [15, 16]. The near-constant efficiency of OB-MIPMB indicates that imprinting-derived recognition sites dominate binding, ensuring robust performance regardless of pH [13]. Such stability is advantageous for wastewater treatment, where effluent pH varies, and has been reported for other lignocellulose-based MIP adsorbents [6].

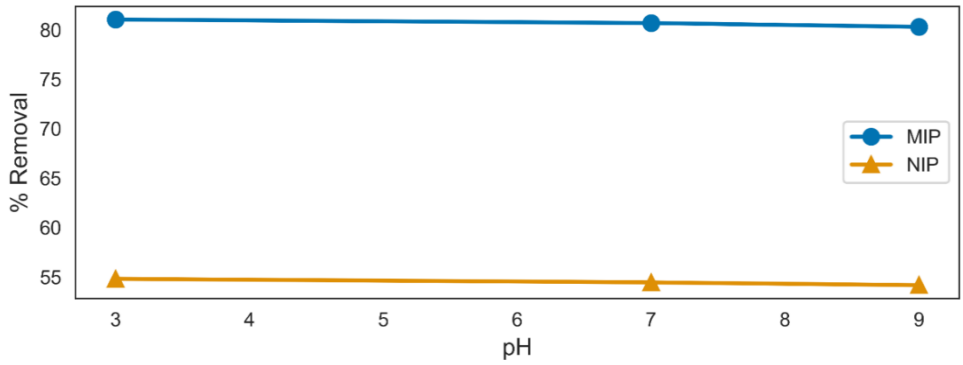

Figure 8. *Effect of pH on MB adsorption.*

Table 1. *Effect of Operational Parameters on Methylene Blue Removal Efficiency.*

Parameter	Condition	OB-MIPM Removal (%)	OB-NIP Removal (%)
Contact Time (min)	0	50.00	50.00

Parameter	Condition	OB-MIPM Removal (%)	OB-NIP Removal (%)
	15	80.68	54.46
	30	81.00	56.56
	45	81.34	57.22
	60	81.64	57.78
	75	81.94	58.28
	90	82.22	58.80
	105	82.78	59.18
	120	83.16	59.42
Adsorbent Dosage (g)	0.05	80.12	54.20
	0.10	80.70	54.46
	0.15	81.58	55.10
	0.20	81.94	55.52
	0.25	82.40	55.98
Initial Concentration (mg/L)	20	97.12	71.35
	40	88.70	67.90
	60	84.08	62.88
	80	74.64	60.59
	100	68.73	58.73
Temperature (℃)	30	80.70	56.46
	40	80.26	55.54
	50	79.90	55.02
	60	79.62	54.60
	70	79.34	54.26
pH	3	81.06	54.82
	7	80.70	54.46
	9	80.32	54.18

3.3. Adsorption Isotherm

Equilibrium adsorption data were fitted to Langmuir, Freundlich, and Temkin models (Table 2; Figures 9-10). The Freundlich model gave the best fit for both OB-MIPMB (R^2 = 0.993) and OB-NIP (R^2 = 0.997), indicating adsorption on a heterogeneous surface with sites of varying affinities [21, 22]. Langmuir analysis yielded a maximum adsorption capacity (Qmax) of 14.93 mg g^{-1} for OB-MIPMB versus 10.26 mg g^{-1} for OB-NIP, confirming the contribution of template-derived recognition sites. The higher Freundlich constant (KF = 4.603 vs. 0.851) also supports stronger dye-polymer interactions in the MIP. The Langmuir separation factor (RL) values for both adsorbents were between 0 and 1, with OB-MIPMB showing a lower RL (0.070) than OB-NIP (0.465), confirming favorable and more efficient adsorption. Temkin analysis suggested weak electrostatic and hydrogen-bonding interactions, consistent with physical adsorption processes inferred from thermodynamic studies [21, 23]. Overall, the results show that molecular imprinting enhances both capacity and affinity, while adsorption is best described by the Freundlich model, consistent with other biomass-derived adsorbents for cationic dyes [22, 23].

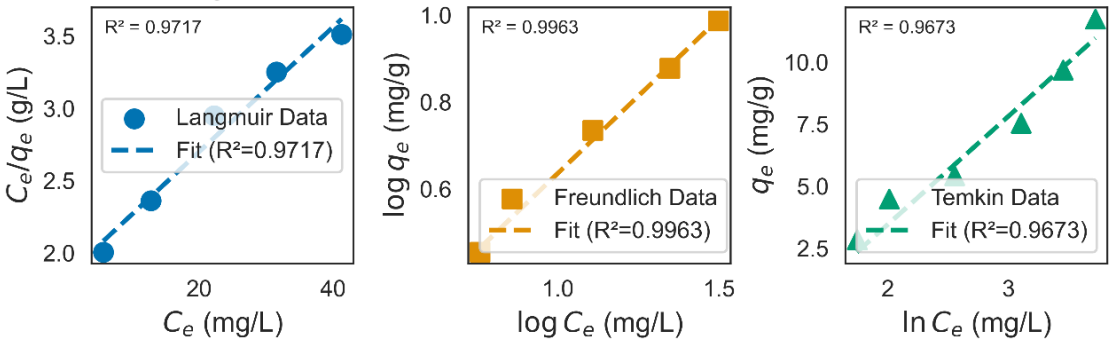

(a) (b) (c)

Figure 9. *Adsorption isotherm plots for methylene blue adsorption on OB-MIPBM (a) Langmuir (b) Freundlich (c) Temkin.*

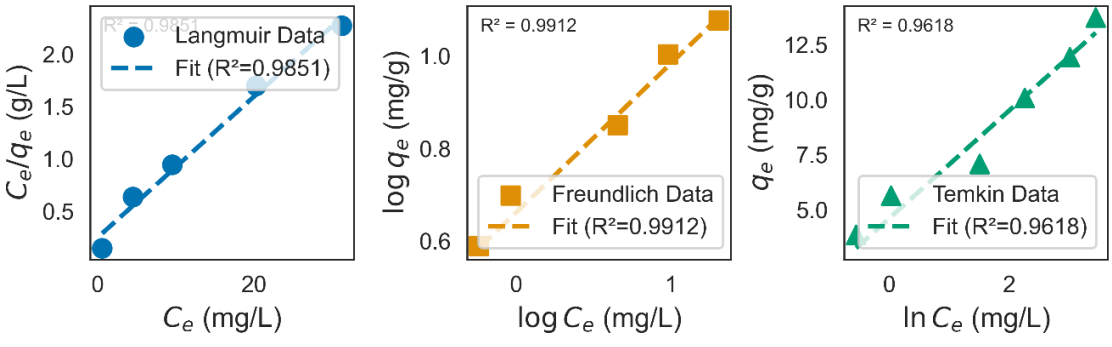

(a) (b) (c)

Figure 10. *Adsorption isotherm plots for methylene blue adsorption on OB-NIP (a) Langmuir (b) Freundlich (c) Temkin.*

Table 2. *Adsorption Isotherm Model Parameters for MB Adsorption.*

Isotherm Model	Parameter	Unit	OB-MIP	OB-NIP
Langmuir	Q_{max}	(mg/g)	14.930	10.26
	R_L		0.070	0.465
	K_L	(L/mg)	0.269	0.023
	R^2	-	0.985	0.971
Freundlich	K_F	$\{mg/g(L/mg)\}^{1/n}$	4.603	0.851
	n	-	3.125	1.414
	R^2	-	0.993	0.997
Temkin	B_T	(J/mol)	6.445	4.367
	K_T	(L/mg)	5.138	1.510
	R^2	-	0.961	0.967

3.4. Adsorption Kinetics

Kinetic modeling (Table 3; Figures 11-12) showed that the second-order model better described MB adsorption on both OB-MIPMB and OB-NIP compared with the first-order model ($R^2 \approx 0.999$). This suggests that adsorption depends on site availability and dye concentration, consistent with

stronger binding interactions in OB-MIPMB. The higher equilibrium capacity of OB-MIPMB (8.40 mg g^{-1}) relative to OB-NIP (6.06 mg g^{-1}) reflects the contribution of template-derived recognition sites. Comparable findings, where second-order kinetics outperform first-order in describing MB adsorption, have been reported for biomass and activated carbon adsorbents [24-26].

The intra-particle diffusion model revealed a two-phase process: rapid surface uptake followed by slower pore diffusion. Non-zero intercepts indicated that boundary-layer resistance also influenced uptake, confirming that diffusion was not the sole rate-limiting factor.

The apparent activation energy (Ea ≈ 18 kJ mol^{-1}) for OB-MIPMB is within the typical range for physical adsorption (<40 kJ mol^{-1}) but lower than reported values for conventional activated carbons (≈33-35 kJ mol^{-1}), suggesting facilitated uptake by imprinted binding sites [27].

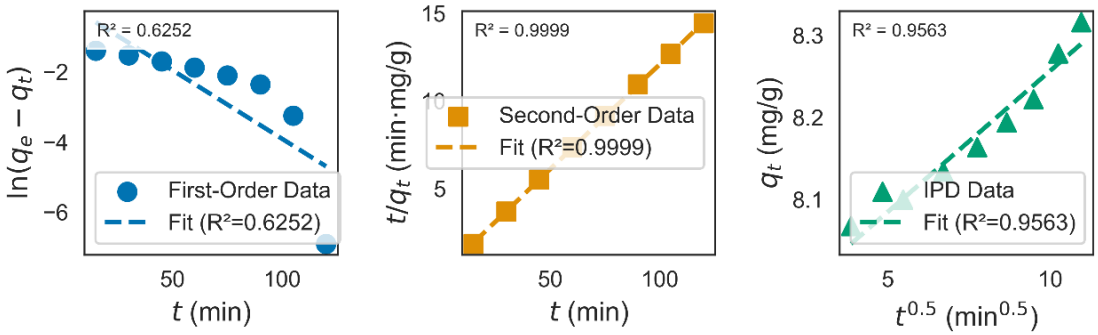

(a) (b) (c)

Figure 11. *Kinetic model plots for methylene blue adsorption on OB-MIPMB (a) First-Order (b) Second-Order (c) Intra-Particle Distribution.*

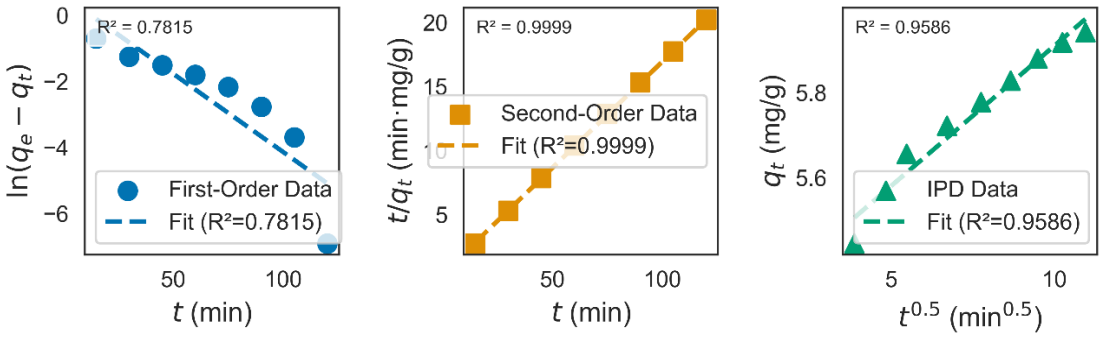

(a) (b) (c)

Figure 12. *Kinetic model plots for methylene blue adsorption on OB-NIP (a) First-Order (b) Second-Order (c) Intra-Particle Distribution.*

Table 3. *Kinetic Model Parameters for MB Adsorption.*

Kinetic Model	Parameter	Unit	OB-MIPMB	OB-NIP
First-Order	k_1	(min^{-1})	0.039	0.047
	R^2	-	0.625	0.781
	Q_e (exp)	(mg/g)	8.317	5.943
	Q_e (Cal)	(mg/g)	0.022	1.645
Second-Order	k_2	g mg^{-1} min^{-1}	0.117	0.078
	R^2	-	0.999	0.999
	Q_e (exp)	(mg/g)	8.317	5.943
	Q_e (Cal)	(mg/g)	8.403	6.061

Kinetic Model	Parameter	Unit	OB-MIPMB	OB-NIP
Intra-particle Diffusion	K_{id}	$mg.g^{-1}min^{-1}$	27.820	14.560
	R^2	-	0.956	0.958
	C	-	-219.800	-76.180

3.5. Thermodynamic Analysis

Thermodynamic parameters (Table 4; Figures 13-14) further clarified the adsorption mechanism. Negative ΔG values across all tested temperatures confirmed the spontaneous nature of MB adsorption on both OB-MIPMB (-36.05 to -37.06 kJ mol^{-1}) and OB-NIP (-4.51 to -5.80 kJ mol^{-1}), with the greater magnitude for OB-MIPMB indicating stronger affinity and more favorable energetics. Similar spontaneous MB adsorption has been reported in other biomass-derived adsorbents [25, 26].

The negative ΔH values (-18.20 kJ mol^{-1} for MIP; -13.87 kJ mol^{-1} for NIP) indicate exothermic adsorption, consistent with the observed decline in uptake at elevated temperatures. The magnitudes fall within the range typically associated with physisorption (<40 kJ mol^{-1}), though the slightly higher value in OB-MIPMB suggests additional stabilization from weak site-specific interactions [24, 27].

Entropy changes highlighted differences between the systems. The positive ΔS for OB-MIPMB (+58.61 J mol^{-1} K^{-1}) suggests increased randomness at the solid-liquid interface, likely from displacement of water molecules during dye binding at recognition sites. In contrast, the negative ΔS for OB-NIP (-26.19 J mol^{-1} K^{-1}) indicates a more ordered state, reflecting nonspecific binding on homogeneous surfaces. Comparable thermodynamic profiles—spontaneous, exothermic, and entropy-driven adsorption—have been reported for MB removal using molecularly imprinted and biomass-based adsorbents [26, 22].

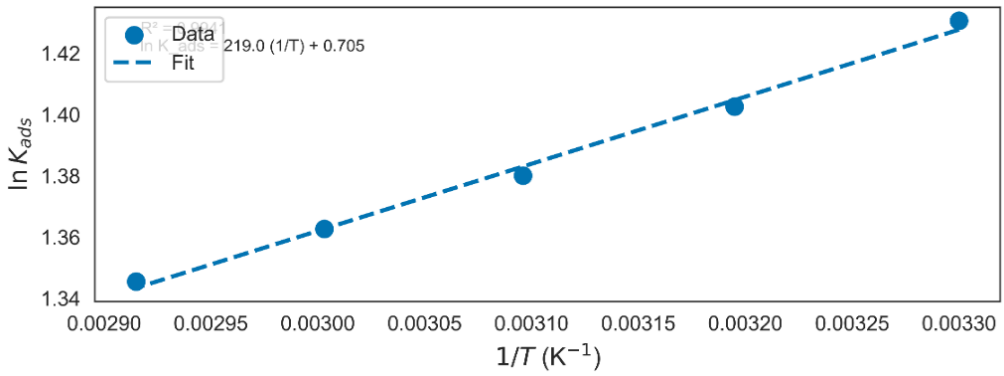

Figure 13. *Van't hoff plot for adsorption of MB on OB-MIPMB.*

Table 4. *Thermodynamic parameters for MB adsorption.*

	OB-MIPBM			OB-NIP		
T (K)	**Δ*G*° (KJ/mol)**	**Δ*H*° (KJ/mol)**	**Δ*S*° (J/mol.K)**	**Δ*G*° (KJ/mol)**	**Δ*H*° (KJ/mol)**	**Δ*S*° (J/mol.K)**
303	-3.605			-0.451		
313	-3.650	-1.652	6.835	-0.579	-0.080	1.344
323	-3.706			-0.541		
333	-3.774			-0.511		
343	-3.838			-0.487		

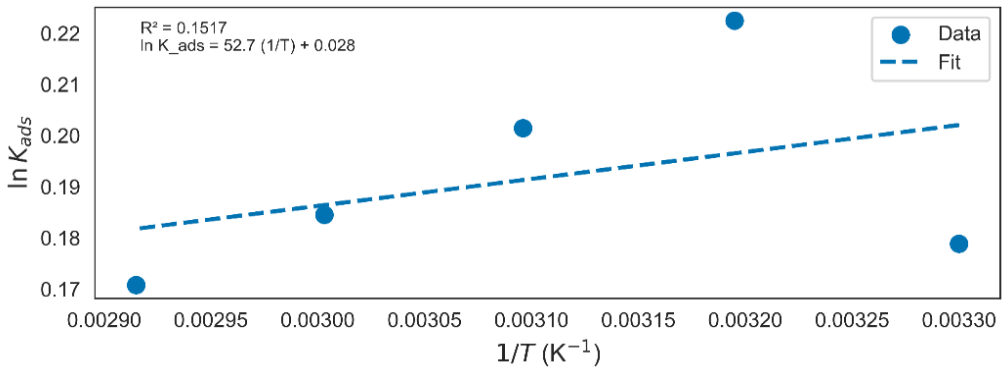

Figure 14. *Van't Hoff plot for MB adsorption on OB-NIP.*

3.6. Selectivity Studies

OB-MIPMB's selectivity was assessed against MB, indigo carmine, and fuchsin basic (50 mg L^{-1}, pH 7, 25 ℃, 10 mg adsorbent; Figure 14, Table 5). For indigo carmine and fuchsin basic, imprinting factors were close to unity (0.992 and 0.9998), and adsorption efficiencies (60.4% and 63.31%) were similar to OB-NIP, indicating nonspecific binding due to structural dissimilarity with MB. By contrast, MB showed a much higher imprinting factor (3.371) and strong selectivity factors (α = 3.245 vs. indigo carmine; α = 2.891 vs. fuchsin basic), confirming that the imprinted cavities were complementary to MB's cationic thiazine structure. Comparable studies have shown that MIPs designed for MB exhibit high template selectivity, while cross-reactivity toward structurally dissimilar dyes remains negligible [28-30].

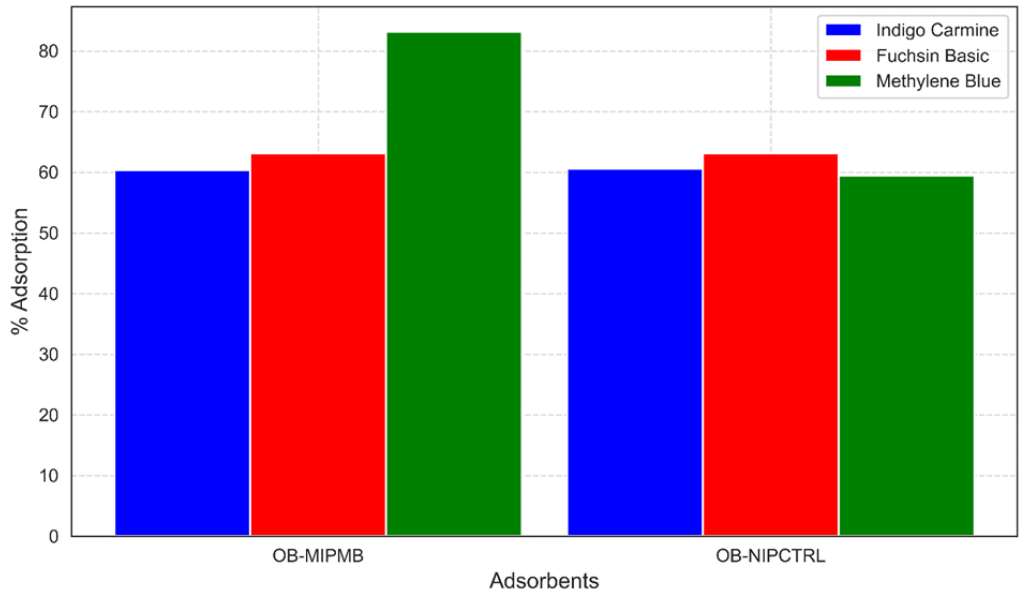

Figure 15. *Adsorption of MB, indigo carmine, and fuchsin basic on OB-MIPMB and OB-NIP.*

Table 5. *Selectivity and imprinting factors for MB, indigo carmine, and fuchsin basic.*

Dye	$Adsorbent$	$qe\ (mg/g)$	$Kd\ (L/g)$	(IF)	$\alpha(MB/dye)$
Indigo Carmine	OB-MIPMB	29.911	3.804	0.992	3.245
Indigo Carmone	OB-NIP	29.864	3.834	-	0.955
Fuchsin Basic	OB-MIPMB	29.1145	4.270	0.9998	2.891

Dye	$Adsorbent$	$qe\ (mg/g)$	$Kd\ (L/g)$	(IF)	$\alpha(MB/dye)$
Fuchsin Basic	OB-NIP	29.113	4.271	-	0.857
Methylene Blue	OB-MIPMB	103.95	12.345	3.371	-
Methylene Blue	OB-NIP	74.275	3.661	-	-

4. Conclusion

This study successfully synthesized cellulose-based molecularly imprinted polymers (MIPs) from oil bean seed shells for the selective removal of methylene blue (MB). Characterization (FTIR, SEM, and XRD) confirmed the formation of template-specific cavities, while batch adsorption experiments showed that OB-MIPMB outperformed the non-imprinted control, achieving a higher adsorption capacity (14.93 mg g^{-1} vs. 10.26 mg g^{-1}). Adsorption followed the second-order kinetic model and was best described by the Freundlich isotherm, consistent with site-specific binding on heterogeneous surfaces. Thermodynamic analysis confirmed that the process was spontaneous and exothermic, with favorable entropy changes in MIP arising from template-derived recognition. Selectivity studies further demonstrated strong molecular recognition for MB, with imprinting and selectivity factors exceeding 3. Although the maximum capacity of OB-MIPMB is modest compared with engineered carbons, its high selectivity, reusability, and the valorization of agro-waste highlight its promise as a sustainable adsorbent for wastewater treatment. Future work should focus on regeneration studies, scale-up of the synthesis, and application in continuous-flow systems to assess industrial feasibility.

Abbreviations

MB	Methylene Blue
MIP	Molecularly Imprinted Polymer
NIP	Nom-imprinted Polymer
FTIR	Fourier Transform Infrared
SEM	Scanning Electron Microscopy
XRD	X-ray Diffraction
NaOH	Sodium Hydroxide
APS	Ammonium Persulphate
AA	Acrylic Acid
AM	Acrylamide
MBA	N,N' – methylenebisacrylamide
H_2O_2	Hydrogen Peroxide
OB-MIPMB	Oil Bean Molecularly Imprinted Polymer for Methylene Blue
OB-NIP	Oil Bean Non-imprinted Polymer
UV-Vis	Ultraviolet-Visible

Acknowledgments

The authors gratefully acknowledge the Department of Pure and Industrial Chemistry, Chukwuemeka Odumegwu Ojukwu University, Uli, Department of Chemistry, Admiralty University of Nigeria, Ibusa, and Department of Chemistry Federal UniooCollins0009versity of Technology, Owerri for providing laboratory facilities and technical support.

Author Contributions

Chinyere Emmanuella Okafor: Conceptualization, Methodology, Investigation, Supervision, Writing – original draft, Writing – review & editing

Collins Chinonso Osuagwu: Conceptualization, Methodology, Writing – original draft

Ekene Chidozie: Formal Analysis, Writing – review & editing

Nnaemeka John Okorocha: Data Curation

Cynthia Chimaobi Onyeakazi: Writing – review & editing

Obi Justina Nnenna: Writing – review & editing

Anyiam Chiemelie Joel: Data Curation

Robert Enenmuo: Investigation, Supervision

Funding

This research received no specific grant from any funding agency in the public, commercial, or not-for-profit sectors.

Data Availability Statement

All data generated or analyzed during this study are included in this published article. Additional data are available from the corresponding author on reasonable request.

Conflicts of Interest

The authors declare no conflicts of interest.

References

[1] Olivito, F., Algieri, V., Jiritano, A., Tallarida, M. A., Tursi, A., Costanzo, P., Maiuolo, L., & De Nino, A. (2021). Cellulose citrate: A convenient and reusable bio-adsorbent for effective removal of methylene blue dye from artificially contaminated water. *RSC Advances*, *11*, 34309-34318. https://doi.org/10.1039/D1RA05464C

[2] Hamad, H. N., & Idrus, S. (2022). Recent developments in the application of bio-waste-derived adsorbents for the removal of methylene blue from wastewater: A review. *Polymers*, *14*(4), 783. https://doi.org/10.3390/polym14040783

[3] Metwally, M. G., Benhawy, A. H., Khalifa, R. M., El Nashar, R. M., & Trojanowicz, M. (2021). Application of molecularly imprinted polymers in the analysis of waters and wastewaters. *Molecules*, *26*(21), 6515. https://doi.org/10.3390/molecules26216515

[4] Gkika, D. A., Tolkou, A. K., Lambropoulou, D. A., Bikiaris, D. N., Kokkinos, P., Kalavrouziotis, I. K., & Kyzas, G. Z. (2024). Application of molecularly imprinted polymers (MIPs) as environmental separation tools. *RSC Applied Polymers*, *2*, 127-148. https://doi.org/10.1039/D3LP00203A

[5] Ahmed, I. M., Ahmed, S., Fouad, Z., Saleh, A. M., Alsalme, A., Bechelany, M., & Barhoum, A. (2024). Fabrication of cellulose nanocrystals/carboxymethyl cellulose/zeolite membranes for methylene blue dye removal: Understanding factors, adsorption kinetics, and thermodynamic isotherms. *Frontiers in Chemistry*, *12*, 1330810. https://doi.org/10.3389/fchem.2024.1330810

[6] Quinto, M. L., Khan, S., Vega-Chacón, J., Mortari, B., Wong, A., Taboada Sotomayor, M. D. P., & Picasso, G. (2023). Development and characterization of a molecularly imprinted polymer for the selective removal of brilliant green textile dye from river and textile industry effluents. *Polymers*, *15*(18), 3709. https://doi.org/10.3390/polym15183709

[7] González-Fernández, L. A., Mizaikoff, B., Medellín-Castillo, N. A., Vilasó-Cadre, J. E., Reyes-Domínguez, I. A., Díaz de León-Martínez, L., Huber, A., & Sánchez-Polo, M. (2025). Molecularly imprinted polymers for pollutant capture and degradation: A snapshot review. *Processes*, *13*(4), 1086. https://doi.org/10.3390/pr13041086

[8] Okafor, C. E., Onyido, I (2022). Comparative adsorptive behaviour of cow dung ash and starch as potential eco-friendly matrices for controlled organophosphorus pesticides delivery. *Scientific Reports* 12, 11169. https://doi.org/10.1038/s41598-022-15292-6

[9] Lazar, M. M., Damaschin, R. P., Volf, I., & Dinu, M. V. (2024). Deep cleaning of crystal violet and methylene blue dyes from aqueous solution by dextran-based cryogel adsorbents. *Gels*, *10*(9), 546. https://doi.org/10.3390/gels10090546

[10] Okwuego, P. O., Okafor, E. C., Okolo, A. J., & Anyanwu, C. G. (2025). Comparative Study of Engineered Bio-Sorbents Derived from Agricultural Waste. *International Journal of Research and Innovation in Applied Science (IJRIIAS) ISSN NO. 2454-6194 https://doi.org/org/10.51584/IJRIAS Vol. 5. Issue, 4.*

[11] Liu, X., Yang, R., Xu, M., Ma, C., Li, W., Yin, Y., Huang, Q., Wu, Y., Li, J., & Liu, S. (2018). Cellulose-based superabsorbent hydrogels crosslinked with acrylic acid and acrylamide for dye removal. *Polymers*, *10*(7), 702. https://doi.org/10.3390/polym10070702

[12] Azizi, A., & Bottaro, C. S. (2020). A critical review of molecularly imprinted polymers for the analysis of organic pollutants in environmental water samples. *Journal of Chromatography A*, *1614*, 460603. https://doi.org/10.1016/j.chroma.2019.460603

[13] Villarreal-Lucio, D. S., Vargas-Berrones, K. X., Díaz de León-Martínez, L., & Flores-Ramírez, R. (2022). Molecularly imprinted polymers for environmental adsorption applications. *Environmental Science and Pollution Research*, *29*, 89923-89942. https://doi.org/10.1007/s11356-022-24025-1

[14] Zhao, B., Jiang, H., Lin, Z., Xu, S., Xie, J., & Zhang, A. (2019). Preparation of acrylamide/acrylic acid cellulose hydrogels for the adsorption of heavy metal ions. *Carbohydrate Polymers*, *224*, 115022. https://doi.org/10.1016/j.carbpol.2019.115022

[15] Shokri, R., Khaledian, M., & Hosseinzadeh, H. (2022). A kinetic and isotherm study on removing methylene blue from aqueous solutions by oxidized cellulose nanostructure. *Emergent Materials*, *5*(5), 1205-1218. https://doi.org/10.1007/s42247-022-00397-5

[16] Zhang, L., Zhou, Y., Wang, J., & Gao, B. (2022). Engineered superabsorbent nanocomposites reinforced with cellulose nanocrystals for remediation of basic dyes: Isotherm, kinetic, and thermodynamic studies. *Polymers*, *14*(3), 567. https://doi.org/10.3390/polym14030567

[17] Rahmawati, A., Nugraheni, A., & Budi, W. S. (2022). Synthesis and adsorption of alginate and starch-based hydrogels for cationic dye removal: Thermodynamic and isotherm modeling. *Indonesian Journal of Chemistry*, *22*(5), 1155-1167. https://doi.org/10.22146/ijc.86908

[18] Venkatram, S., McCollum, J., Stingelin, N., & Brettmann, B. (2023). A close look at polymer degree of crystallinity versus polymer crystalline quality. *Polymer International*, *72*(10), 855-860. https://doi.org/10.1002/pi.6508

[19] Poopakdee, N., & Thammawichai, W. (2024). The effects of the crystallinity index of cellulose on the flexural properties of hybrid-cellulose epoxy composites. *Journal of Metals, Materials and Minerals*, *34*(3), 1902. https://doi.org/10.55713/jmmm.v34i3.1902

[20] Hasani, M., Sedaghatzadeh, A., Ghaedi, M., & Jannesar, R. (2022). Theoretical, equilibrium, kinetics and thermodynamic study of adsorption of methylene blue onto coal. *Molecules*, *27*(6), 1856. https://doi.org/10.3390/molecules27061856

[21] Shoaib, M., Bukhari, S. N. A., Ibrahim, M., Khalid, H., & Danish, M. (2024). Starch-grafted-poly(acrylic acid)/Pterocladia capillacea composite for efficient methylene blue adsorption: Equilibrium, kinetics, and thermodynamics. *Biomass Conversion and Biorefinery*, *14*, 1837-1852. https://doi.org/10.1007/s13399-022-03382-4

[22] Siddiqui, S. H., Uddin, M. K., Isaac, R., & Aldosari, O. F. (2022). An effective biomass for the adsorption of methylene blue dye and treatment of river water. *Adsorption Science & Technology, 2022*, 4143138. https://doi.org/10.1155/2022/4143138

[23] Liyanaarachchi, H., Thambiliyagodage, C., Lokuge, H., & Vigneswaran, S. (2023). Kinetics and thermodynamics study of methylene blue adsorption to sucrose- and urea-derived nitrogen-enriched, hierarchically porous carbon activated by KOH and H_3PO_4. *ACS Omega*, *8*(18), 16158-16169. https://doi.org/10.1021/acsomega.3c00339

[24] Abbas, M., & Trari, M. (2024). Adsorption behavior of methylene blue onto activated coconut shells: Kinetic, thermodynamic, mechanism and regeneration of the adsorbent. *Dose-Response*, *22*(4), 15593258241290708. https://doi.org/10.1177/15593258241290708

[25] Mian, I., Escalante, J., & Rodr ǵuez, R. (2022). Removal of methylene blue from wastewater using activated carbon prepared from biomass: Adsorption and thermodynamic studies. *Journal of the Mexican Chemical Society*, *66*(4), 507-516. https://doi.org/10.29356/jmcs.v66i4.1688

[26] Asman, S., Yusof, N. A., Abdullah, A. H., & Haron, M. J. (2012). Synthesis and characterization of hybrid molecularly imprinted polymer (MIP) membranes for removal of methylene blue (MB). *Molecules*, *17*(2), 1916-1928. https://doi.org/10.3390/molecules17021916

[27] Inamullah, M., Alam, S., Rehman, N., & Ullah, H. (2022). Utilization of biomass (Eucalyptus lanceolata) as an adsorbent - Removal of methylene blue from wastewater. *Journal of the Mexican Chemical Society*, *66*(4). https://doi.org/10.29356/jmcs.v66i4.1667

[28] Kondo, T., Sawatari, C., & Wada, M. (2021). Novel terahertz spectroscopy technology for crystallinity and crystal structure analysis of cellulose. *Polymers*, *13*(1), 6. https://doi.org/10.3390/polym13010006

[29] Sadia, M., Ahmad, I., Ali, F., Zahoor, M., Ullah, R., Khan, F. A., Ali, E. A., & Sohail, A. (2022). Selective removal of the emerging dye Basic Blue 3 via molecularly imprinting technique. *Molecules*, *27*(10), 3276. https://doi.org/10.3390/molecules27103276

[30] Sedelnikova, A., Poletaeva, Y., Golyshev, V., Chubarov, A., & Dmitrienko, E. (2023). Preparation of magnetic molecularly imprinted polymer for methylene blue capture. *Magnetochemistry*, *9*(8), 196. https://doi.org/10.3390/magnetochemistry9080196